Brownian Motion of Boomerang Colloidal Particles

Ayan Chakrabarty,[1] Andrew Konya,[1] Feng Wang,[1] Jonathan V. Selinger,[1,†] Kai Sun,[2] and Qi-Huo Wei[1,*]

[1]*Liquid Crystal Institute, Kent State University, Kent, Ohio 44242, USA*

[2]*Department of Materials Science and Engineering, University of Michigan, Ann Arbor, Michigan 48109, USA*

(Received 5 March 2013; revised manuscript received 2 August 2013; published 18 October 2013)

We investigate the Brownian motion of boomerang colloidal particles confined between two glass plates. Our experimental observations show that the mean displacements are biased towards the center of hydrodynamic stress (CoH), and that the mean-square displacements exhibit a crossover from short-time faster to long-time slower diffusion with the short-time diffusion coefficients dependent on the points used for tracking. A model based on Langevin theory elucidates that these behaviors are ascribed to the superposition of two diffusive modes: the ellipsoidal motion of the CoH and the rotational motion of the tracking point with respect to the CoH.

DOI: 10.1103/PhysRevLett.111.160603 PACS numbers: 05.40.Jc, 47.57.J−, 66.10.C−, 82.70.Dd

Brownian motion as a general phenomenon of diffusion processes has inspired extensive research [1–12] due to both its interesting physics and practical applications such as in microrheology [13–16], self-propelled microswimmers [17] and particle and molecular separation [18–20]. Inspired by the diverse geometric shapes of biological macromolecules, Brenner and others have extended the hydrodynamic theory of Brownian motion to particles with irregular shapes [21–27]. A set of hydrodynamic centers are introduced, which include the center of hydrodynamic stress (CoH) where the coupling diffusion matrix becomes zero, the center of reaction where the coupling resistance matrix becomes symmetric and the center of diffusion where the coupling diffusion matrix becomes symmetric [22,24,28]. For screwlike or skewed particles, the translational and rotational motions are intrinsically coupled; therefore, the CoH does not exist and the centers of diffusion and reaction differ from each other. By contrast, for nonskewed particles, there always exists a unique point at which these three hydrodynamic centers coincide.

Thus far, experimental studies on Brownian motion have been focused primarily on spherical particles; it was only recently that the Brownian motion of low-symmetry particles was explored in experiments [5,29–37]. Particle shapes are critical to various applications such as self-propelled microswimmers and particle or molecular separations [17,38]. By engineering particle shapes, microswimmers may be tailored to perform circular, spinning-top, or other types of motion [38–40]. Understanding the hydrodynamics of chiral particles may lead to new avenues towards separation of particle or molecular enantiomers [41].

In this Letter we study the Brownian motion of boomerang-shaped colloidal particles under quasi-two-dimensional (2D) confinements. The boomerang particles with C_{2v} mirror symmetry represent an attractive system for studying the Brownian motion of low symmetry particles because their center of mass and CoH do not coincide and both lie outside the body. Especially, the location of the CoH is unknown before the motion of any tracking point (TP) is analyzed. Boomerang particles may also serve as a model system for active microswimmers [40], the electro-optical properties of DNA molecules [42–45], and liquid crystalline ordering [46].

Our experimental and theoretical studies show that the diffusion of the boomerangs is rather different from that of spheres and ellipsoids. (i) The mean displacements (MD) for fixed initial angle are biased towards the CoH, and the mean square displacements (MSDs) exhibit a crossover from short- to long-time diffusion with different diffusion coefficients. (ii) The boomerangs confined in quasi-2D are nonskewed and possess a CoH where translation and rotation are decoupled in the body frame. (iii) Our model based on Langevin theory shows that the nonzero MDs result from the Brownian orbital motion of the TP with respect to the CoH. (iv) Two methods for calculating body frame displacements which give indistinguishable results for ellipsoids, yield drastically different results for boomerang particles.

The boomerang colloidal particles made of photocurable polymer (SU8) were fabricated by using photolithography [47] and have a 2.1 μm arm length, 0.51 μm thickness, 0.55 μm arm width, and a 90° apex angle [Fig. 1(a)]. The aqueous suspension of the particles, stabilized by adding sodium dodecyl sulfate, (SDS, 1mM) was filled in a cell of $\sim$2 μm thickness. Videos of isolated moving boomerangs were taken using a CCD camera at time step $\tau = 0.05$ s. Limited by the computer memory, each video contains 3000 frames and a total of 167 videos were taken for the same particle.

We developed an image processing algorithm to track the position and orientation of the boomerang particles. The cross point between the central axes of the two arms represents the center of the body (CoB) and is a convenient point for motion tracking. The angle bisector gives the particle orientation θ [Fig. 1(b)]. The precision of our optical microscope and tracking algorithm is determined

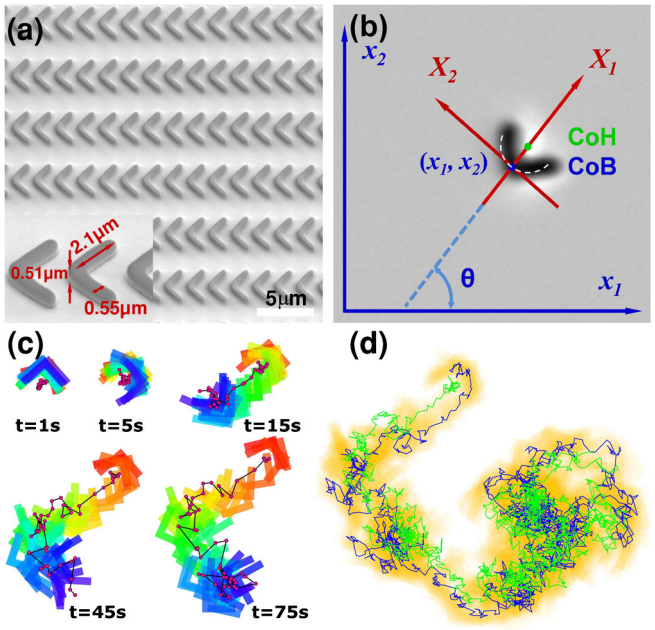

FIG. 1 (color online). (a) SEM image of the boomerang particles fabricated on a silicon wafer. (b) Optical microscopic image and schematics of the coordinate systems. $(x_1 - x_2)$ is the lab frame and $(X_1 - X_2)$ is the body frame. (c) Representative trajectories of 5 different total lengths of time, where the red spots represent the positions of the CoH, and the boomerang is colored-coded in time. (d) An exemplary 300 s trajectory for the CoH (green) and the CoB (blue).

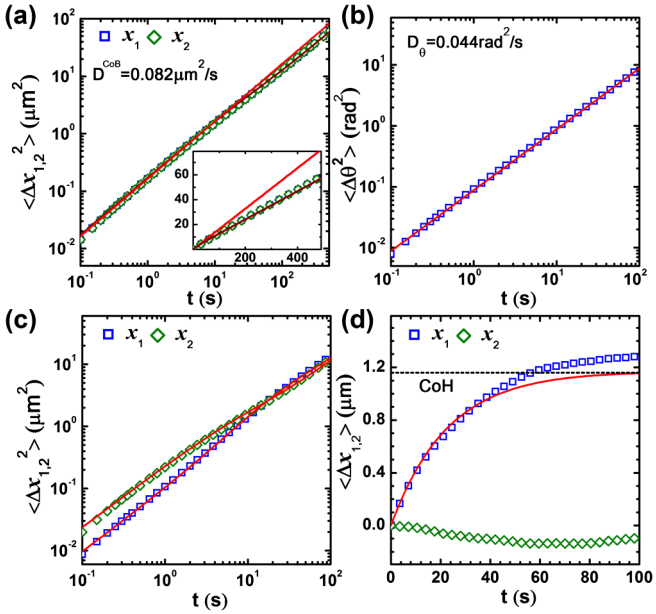

FIG. 2 (color online). (a) MSDs of the CoB in the lab frame vs. t. Red line: the best linear fit for $t < 10$ s; dark brown line: theoretical fit using Eq. (2). Inset: linear plot of MSDs vs. t. (b) MSDs of θ vs. t with the best linear fitting (red line). (c) MSDs for the CoB in the lab frame with $\theta_0 = 0$. Red lines: theory curves with Eq. (1b). (d) MDs in the lab frame with $\theta_0 = 0$. Red line: theory curve of Eq. (1a) using D_θ and $D_{2\theta}$ obtained from Fig. 2(b) and 3(e).

to be ± 13 nm and ± 0.004 rad for position and orientation, respectively. Trajectories obtained from all videos were merged into a single trajectory of $\sim 5 \times 10^5$ frames. To merge two trajectories together, the particle coordinates in the second video are shifted and rotated such that the position and orientation of the first frame in the second video matches those of the last frame in the first video. Figures 1(c) and 1(d) show representative trajectories of the CoB and CoH at different time scales where the coupling between translational and rotational motions can be easily observed (the method to locate the CoH will be discussed later).

In Fig. 2(a), the angle averaged MSDs of the CoB along x_1 and x_2 are identical, implying that the Brownian motion is isotropic on average. In contrast to the MSDs for ellipsoids that grow linearly with time, the MSDs for the boomerangs exhibit linearity with time only in short and long times with a nonlinear crossover region around $t = 10$ s. Best linear fittings give the short- and long-time diffusion coefficients, respectively, as $\bar{D}^{\mathrm{ST}} = 0.082\ \mu\mathrm{m}^2/\mathrm{s}$, $\bar{D}^{\mathrm{LT}} = 0.057\ \mu\mathrm{m}^2/\mathrm{s}$. In Fig. 2(b), the rotational Brownian motion is linear at all times $\langle[\Delta\theta(t)]^2\rangle = 2D_\theta t$, with the diffusion coefficient $D_\theta = 0.044\ \mathrm{rad}^2/\mathrm{s}$.

To discern anisotropic features in the Brownian motion, we measured the MSDs with the initial angle fixed at $\theta_0 = 0$. Because of its anisotropic shape, the MSDs at short times exhibit different diffusion coefficients along x_1 and x_2. At long times when the directional memory is washed out, the MSDs grow again linearly with t with identical slope for both x_1 and x_2 [Fig. 2(c)]. To note, the MSDs along x_1 is larger than that along x_2 at long times, while they are identical for ellipsoids [5].

Although the MDs for Brownian motion are typically zero, we find that it is not the case for the boomerangs. The MDs averaged over different initial angle θ_0 are indeed zero (data not shown here). However, with initial angle fixed at $\theta_0 = 0$, the MDs along x_1 are nonzero [Fig. 2(d)] and saturate at long times. Such nonzero MDs along the symmetric line are in sharp contrast with the zero MDs observed for spheres and ellipsoids.

To understand these observations, we assume that the boomerangs confined in 2D possess a CoH (as will later be proved experimentally). The position of a TP on the symmetric line can be expressed as $\mathbf{x}(t) = \mathbf{x}^{\mathrm{CoH}}(t) - r\cos\theta(t)\hat{\mathbf{x}}_1 - r\sin\theta(t)\hat{\mathbf{x}}_2$, where $\boldsymbol{r}$ is the vector from the CoH to the TP. When the CoB is used as the TP, we denote the CoB-CoH separation as d_0. From the definition of the CoH, the descriptions of the Brownian motion of the CoH requires only one rotation diffusion coefficient D_θ and two translation diffusion coefficients D_{22}^{CoH} and D_{11}^{CoH}, and therefore the Langevin equations for the CoH are actually the same as those for an ellipsoid. As shown in the Supplemental Material [48], the MDs and MSDs of the TP for fixed initial angle θ_0 can be written as

$$\langle \Delta x_i(t)\rangle_{\theta_0} = r a_i \tau_1(t) \tag{1a}$$

$$\langle [\Delta x_i(t)]^2\rangle_{\theta_0} = 2\bar{D}^{\mathrm{CoH}} t + \cos 2\theta_0 (r^2/2 + \Delta D/4D_\theta) b_i \tau_4(t) + 2r^2 a_i^2 \tau_1(t), \tag{1b}$$

where $\tau_n = 1 - \exp(-nD_\theta t)$, $a_1 = \cos\theta_0$, $a_2 = \sin\theta_0$, $b_1 = -1$, $b_2 = 1$, $\bar{D}^{\mathrm{CoH}} = (D_{11}^{\mathrm{CoH}} + D_{22}^{\mathrm{CoH}})/2$, $\Delta D = D_{22}^{\mathrm{CoH}} - D_{11}^{\mathrm{CoH}}$. Equation (1a) indicates that $\langle \Delta x_1(t)\rangle_{\theta_0}$ for the CoB saturates at $r = d_0$ in the long time, or the Brownian motion is biased towards the CoH. These theoretical expressions agree well with the experimental results [Figs. 2(c) and 2(d)].

Averaging Eq. (1a) and (1b) over different initial angle θ_0 leads to that the angle averaged MDs are zero and the angle-averaged MSDs are expressed as [48]

$$\langle [\Delta x_{1,2}(t)]^2\rangle = 2\bar{D}^{\mathrm{CoH}} t + r^2 \tau_1(t). \tag{2}$$

Here the crossover time of the $\tau_1(t)$ term is determined by the rotational diffusion coefficient, $\tau_\theta = 1/(2D_\theta) = 11$ s. Equation (2) indicates that the short-time diffusion coefficient $\bar{D}^{\mathrm{ST}} = \bar{D}^{\mathrm{CoH}} + r^2 D_\theta/2$ is dependent on the position of the TP, while the long time diffusion coefficient $\bar{D}^{\mathrm{LT}} = \bar{D}^{\mathrm{CoH}}$ is independent of the TP. This expression fits very well the experimental data Fig. 2(a). This crossover has been predicted by previous theory [25,49] and is observed here for the first time in experiments.

This model also shows that the nonzero MDs originate from the Brownian motion of the vector $\boldsymbol{r}$, considering that the motion of the CoB is the superposition of the ellipsoid-like motion of the CoH and the motion of $\boldsymbol{r}$. The Brownian rotation of the vector $\boldsymbol{r}$ results in random displacements of the CoB on an arc centered at the CoH [dashed line in Fig. 1(b)]; the projection of these random orbital displacements is symmetric to the CoB along the X_2 axis while biased on average towards the CoH along the X_1 axis. When this Brownian orbital motion of the CoB covers a circle for $t \gg \tau_\theta$, the MDs saturate and the Brownian motion is dominated by that of the CoH.

To measure the other elements of the diffusion tensor, the translational displacements need to be transformed into a body frame comoving with the particle. One convenient body frame has its origin fixed at the CoB and X_1 axis coincident with the symmetry axis [Fig. 1(b)]. The displacements between consecutive body frames were obtained from those in the lab frame through the rotational transformation $\Delta X_i(\tau, t_n) = R_{ij}(\theta_n)\Delta x_j(\tau, t_n)$, where i, $j = 1$ or 2, and $R_{ij}(\theta_n)$ is the rotation transformation matrix. The body frame trajectories are constructed by accumulating the displacements, $X_i(t_n) = \sum_{k=0}^{n} \Delta X_i(t_k)$.

One has two different choices of θ_n: $\theta_n = \theta(t_n)$ representing the orientation at the beginning of each time interval, or $[\theta(t_n) + \theta(t_{n+1})]/2$ representing the average orientation during the time interval. One previous work shows that these two choices give indistinguishable results for particles of high symmetry such as ellipsoids [5]. However, we find that the distinction between these two frames becomes important for low-symmetry particles such as the boomerangs. We term the first $[\theta_n = \theta(t_n)]$ as the discrete body frame (DBF) and the second $[\theta_n = [\theta(t_n) + \theta(t_{n+1})]/2]$ as the continuous body frame (CBF) [48].

In the CBF, the measured MDs along both the X_1 and X_2 directions are zero [Fig. 3(a)], and the MSDs are linear with time, $\langle [\Delta X_i(t)]^2\rangle = 2D_{ii}t$ with the diffusion coefficients $D_{11} = 0.049\ \mu\mathrm{m}^2/\mathrm{s}$ and $D_{22} = 0.117\ \mu\mathrm{m}^2/\mathrm{s}$ [Fig. 3(c)]. In contrast, very different behaviors are observed in the DBF. While the MD along X_2 is zero, the MD along X_1 is nonzero and grows linearly with time [Fig. 3(b)]. Accompanying this nonzero drift, the MSDs along X_1 exhibit nonlinearity with time [Fig. 3(d)]. Since the orientation of the DBF is reset at the beginning of each time step, the nonzero value of $\langle \Delta X_1\rangle$ seen in the DBF is actually a manifestation of the nonzero MDs $\langle \Delta x_1\rangle$ observed in the lab frame for $\theta_0 = 0$.

Since the displacements of the CoB along X_2 tend to induce rotation and vice versa, the coupled diffusion

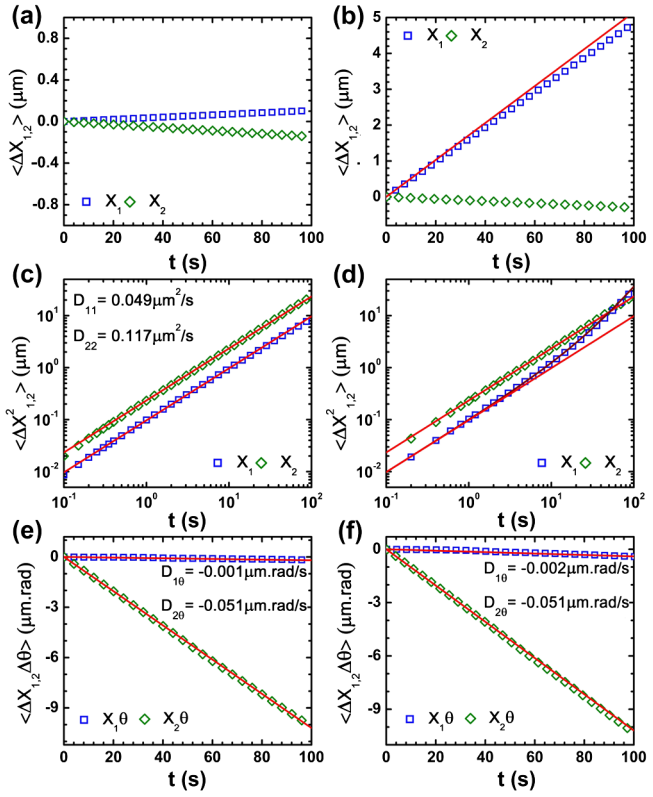

FIG. 3 (color online). (a)–(b) MDs vs t in the CBF (a) and DBF (b). The red line in (b) is the theory curve of Eq. (4a). (c)–(d) MSDs vs t in the CBF (c) and DBF (d). In (c), the red lines are the best linear fittings. In (d), the dark brown curve is Eq. (4b) with D_θ and $D_{2\theta}$ obtained from the data in Fig. 2 and the red straight lines have the same slopes as those in (c). (e)–(f) Translation-rotation correlations vs t in the CBF (e) and DBF (f). The red lines are the best linear fitting.

coefficient $D_{2\theta}$ is nonzero. While the translational motion of the CoB along X_1 is decoupled with rotation, $D_{1\theta}$ is thus zero. Our experimental results show that the DBF and CBF give rise to similar results for the translation-rotation correlation functions [Fig. 3(e) and 3(f)]. Linear fitting of these data with $\langle \Delta X_i(t)\Delta\theta(t)\rangle = 2D_{i\theta}t$ gives a negligible value for $D_{1\theta}(\leq -0.002\ \mu\text{m}\cdot\text{rad/s})$, and $D_{2\theta} = 0.051\ \mu\text{m}\cdot\text{rad/s}$ [Figs. 3(e) and 3(f)].

The differences between the CBF and DBF can be ascribed to the differences between the displacements of the vector $\boldsymbol{r}$ in these two body frames. The first and second moments of displacements for the TP can be expressed in the CBF as [48]

$$\langle \Delta X_1(t)\rangle = \langle \Delta X_2(t)\rangle = 0, \tag{3a}$$
$$\langle \Delta X_1^2(t)\rangle = 2D_{11}t = 2D_{11}^{\text{CoH}}t, \tag{3b}$$
$$\langle \Delta X_2^2(t)\rangle = 2D_{22}t = 2(D_{22}^{\text{CoH}} + r^2 D_\theta)t, \tag{3c}$$

and in the DBF as

$$\langle \Delta X_1(t)\rangle = rD_\theta t; \qquad \langle \Delta X_2(t)\rangle = 0, \tag{4a}$$
$$\langle \Delta X_1^2(t)\rangle = 2D_{11}^{\text{CoH}}t + (rD_\theta)^2 t^2, \tag{4b}$$
$$\langle \Delta X_2^2(t)\rangle = 2D_{22}t = 2(D_{22}^{\text{CoH}} + r^2 D_\theta)t. \tag{4c}$$

The CBF and DBF give the same forms for the translation-rotation correlation functions: $\langle \Delta X_1 \Delta\theta\rangle = 0$, and $\langle \Delta X_2 \Delta\theta\rangle = 2D_{2\theta}t = 2rD_\theta t$ [48]. These theoretical results agree well with the experiments [Fig. 3].

Based on Eq. (1a) and (4a), the slopes of the MDs vs time are the same at short times in the DBF and in the lab frame (for $\theta_0 = 0$), which agrees with the experiments [Figs. 2(d) and 3(b)]. Employing the DBF provides a physical picture consistent with the lab frame observations, while using the CBF averages out the drift terms in MDs and MSDs and provides a convenient way to calculate diffusion coefficients.

To verify the existence of the CoH, we re-calculated the trajectories and the diffusion coefficients for TPs on the symmetry line with its distance from the CoB defined as $d = d_0 - r$. We see that the theoretical expressions of D_{22} and $D_{2\theta}$ as functions of r, $D_{22} = D_{22}^{\text{CoH}} + r^2 D_\theta$, and $D_{2\theta} = rD_\theta$, can fit the experimental results well [Figs. 4(a) and 4(b)]; D_{11} remains unchanged, D_{22} reaches a minimum at $d = 1.16\ \mu$m and $D_{2\theta}$ crosses zero approximately at $1.16\ \mu$m. These indicate that the CoH is at a distance $d_0 = 1.16\ \mu$m from the CoB, which agrees with $D_{2\theta} = d_0 D_\theta$.

With the CoH as TP, the MSDs in the lab and body frames all grow linearly with time and the translation-rotation correlation functions are zero [Fig. S1(a)–(c)]. As expected, the differences between DBF and CBF disappear. The averaged diffusion coefficient for the CoH in the lab frame, $\bar{D}^{\text{CoH}} = 0.054\ \mu\text{m}^2/\text{s}$, agrees with the long-time averaged diffusion coefficient of the CoB.

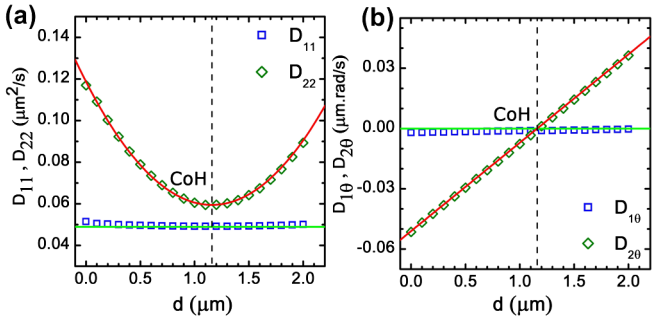

FIG. 4 (color online). (a) D_{11} and D_{22} vs d. Red and green lines are theory curves based on Eqs. (3b) and (3c). (b) $D_{1\theta}$ and $D_{2\theta}$ vs d. Red and green lines are the theory curves of $D_{2\theta} = rD_\theta$ and $D_{1\theta} = 0$, respectively. The dashed lines indicate the CoH at $d_0 = 1.16\ \mu$m.

Theoretical studies have shown that bent rods in 3D are skewed [25], and thus it is not trivial to prove the existence of the CoH for the boomerangs in quasi-2D confinements. In general, particles with only two mutually perpendicular symmetry planes are skewed in 3D [22]. The difference between the 2D and 3D behaviors can be understood as the following: at the CoH, translation in the X_1-X_2 plane is decoupled from the rotation of θ; while at the same point in three dimensions, translation perpendicular to the X_1-X_2 plane is not decoupled from rotation around X_2. Therefore, raising cell thicknesses will lead not only to variations in diffusion coefficients as seen in spherical particles [50–52], but also to qualitatively different behaviors. While our experiments with 1.7 and 1.9 μm thick cells for the same or different boomerang particles show qualitatively similar results, the crossover from the nonskewed 2D behaviors to skewed 3D behaviors is worthy of further detailed studies.

In conclusion, we have shown that the Brownian motion of the boomerang particles exhibits nonzero MDs for fixed initial angles, TP-dependent short-time and TP-independent long-time diffusion coefficients as results of nonoverlap between the TP and its CoH. These results observed in boomerangs should occur in any nonskewed particles as long as the TP is not coincident with the CoH, and thus have important implications for studying the diffusion and transport of anisotropic particles. The subtle difference between the CBF and DBF has significant influence on proper calculations of diffusion coefficients. Prior theoretical studies have provided analytical results regarding the orientation distributions of bent rods under external fields [42–45]; it will be interesting to study how the boomerangs transport under gravitational or electrophoretic forces.

The authors would like to acknowledge Hartmut Löwen, Tom Lubensky, and Kun Zhao for valuable discussions and Oleg Lavrentovich for both valuable discussions and using the equipment in his lab. Partial financial support from NSF Grant No. DMR-1106014, ECCS-0824175, and the Farris Family Award are acknowledged.

*To whom all correspondence should be addressed.
qwei@kent.edu
†jselinge@kent.edu.

[1] A. Einstein, Ann. Phys. (N.Y.) **17**, 549 (1905).
[2] S. Chandrasekhar, Rev. Mod. Phys. **15**, 1 (1943).
[3] P. Hanggi and F. Marchesoni, Chaos **15**, 026101 (2005).
[4] E. Frey and K. Kroy, Ann. Phys. (Berlin) **14**, 20 (2005).
[5] Y. Han, A. M. Alsayed, M. Nobili, J. Zhang, T. C. Lubensky, and A. G. Yodh, Science **314**, 626 (2006).
[6] V. Blickle, T. Speck, C. Lutz, U. Seifert, and C. Bechinger, Phys. Rev. Lett. **98**, 210601 (2007).
[7] B. Wang, S. M. Anthony, S. C. Bae, and S. Granick, Proc. Natl. Acad. Sci. U.S.A. **106**, 15 160 (2009).
[8] D. Rings, R. Schachoff, M. Selmke, F. Cichos, and K. Kroy, Phys. Rev. Lett. **105**, 090604 (2010).
[9] T. C. Li, S. Kheifets, D. Medellin, and M. G. Raizen, Science **328**, 1673 (2010).
[10] T. Franosch, M. Grimm, M. Belushkin, F. M. Mor, G. Foffi, L. Forró, and S. Jeney, Nature (London) **478**, 85 (2011).
[11] R. X. Huang, I. Chavez, K. M. Taute, B. Lukić, S. Jeney, M. G. Raizen, and E.-L. Florin, Nat. Phys. **7**, 576 (2011).
[12] I. Buttinoni, G. Volpe, F. Kümmel, G. Volpe, and C. Bechinger, J. Phys. Condens. Matter, **24**, 284129 (2012).
[13] T. G. Mason and D. A. Weitz, Phys. Rev. Lett. **74**, 1250 (1995).
[14] T. A. Waigh, Rep. Prog. Phys. **68**, 685 (2005).
[15] P. Cicuta and A. M. Donald, Soft Matter **3**, 1449 (2007).
[16] A. Mukhopadhyay and S. Granick, Curr. Opin. Colloid Interface Sci. **6**, 423 (2001).
[17] P. Romanczuk, M. Bär, W. Ebeling, B. Lindner, and L. Schimansky-Geier, Eur. Phys. J. Special Topics **202**, 1 (2012).
[18] J. Rousselet, L. Salome, A. Ajdari, and J. Prostt, Nature (London) **370**, 446 (1994).
[19] C. F. Chou *et al.*, Proc. Natl. Acad. Sci. U.S.A. **96**, 13 762 (1999).
[20] P. Reimann, Phys. Rep. **361**, 57 (2002).
[21] H. Brenner, J. Colloid Sci. **20**, 104 (1965).
[22] H. Brenner, J. Colloid Interface Sci. **23**, 407 (1967).
[23] J. Garcia De La Torre and V. A. Bloomfield, Biopolymers **17**, 1605 (1978).
[24] S. C. Harvey and J. Garcia De La Torre, Macromolecules **13**, 960 (1980).
[25] W. A. Wegener, Biopolymers **20**, 303 (1981).
[26] E. Dickinson, S. A. Allison, and J. A. McCammon, J. Chem. Soc., Faraday Trans. 2 **81**, 591 (1985).
[27] X. Q. Sun, T. Lin, and J. D. Gezelter, J. Chem. Phys. **128**, 234107 (2008).
[28] B. Carrasco and J. G. De La Torre, Biophys. J. **76**, 3044 (1999).
[29] D. Mukhija and M. J. Solomon, J. Colloid Interface Sci. **314**, 98 (2007).
[30] C. Ribrault, A. Triller, and K. Sekimoto, Phys. Rev. E **75**, 021112 (2007).
[31] S. M. Anthony, M. Kim, and S. Granick, J. Chem. Phys. **129**, 244701 (2008).
[32] M. Hoffmann, C. S. Wagner, L. Harnau, and A. Wittemann, ACS Nano **3**, 3326 (2009).
[33] B. H. McNaughton, M. Shlomi, P. Kinnunen, C. Cionca, S. N. Pei, R. Clarke, P. Argyrakis, and R. Kopelman, Appl. Phys. Lett. **97**, 144103 (2010).
[34] M. P. Lettinga, J. K. G. Dhont, Z. Zhang, S. Messlinger, and G. Gompper, Soft Matter **6**, 4556 (2010).
[35] G. L. Hunter, K. V. Edmond, M. T. Elsesser, and E. R. Weeks, Opt. Express **19**, 17 189 (2011).
[36] D. J. Kraft, R. Wittkowski, B. ten Hagen, K. V. Edmond, D. J. Pine, H. Löwen, arXiv:1305.1253.
[37] J. Fung and V. N. Manoharan, Phys. Rev. E **88**, 020302 (2013).
[38] R. Wittkowski and H. Löwen, Phys. Rev. E **85**, 021406 (2012).
[39] J. G. Gibbs, S. Kothari, D. Saintillan, and Y. P. Zhao, Nano Lett. **11**, 2543 (2011).
[40] F. Kümmel, B. ten Hagen, R. Wittkowski, I. Buttinoni, R. Eichhorn, G. Volpe, H. Löwen, and C. Bechinger, Phys. Rev. Lett. **110**, 198302 (2013).
[41] M. Aristov, R. Eichhorn, and C. Bechinger, Soft Matter **9**, 2525 (2013).
[42] W. A. Wegener, Biopolymers **23**, 2243 (1984).
[43] W. A. Wegener, J. Chem. Phys. **84**, 5989 (1986).
[44] J. P. Umazano and J. A. Bertolotto, J. Chem. Phys. **134**, 125107 (2011).
[45] J. P. Umazano and J. A. Bertolotto, J. Chem. Phys. **138**, 095102 (2013).
[46] H. Takezoe and Y. Takanishi, Jpn. J. Appl. Phys. **45**, 597 (2006).
[47] C. J. Hernandez and T. G. Mason, J. Phys. Chem. C **111**, 4477 (2007).
[48] See Supplemental Material at http://link.aps.org/supplemental/10.1103/PhysRevLett.111.160603 for detailed theoretical derivations and measurement data for the CoH.
[49] B. Cichocki, M. L. Ekiel-Jezewska, and E. Wajnryb, J. Chem. Phys. **136**, 071102 (2012).
[50] L. P. Faucheux and A. J. Libchaber, Phys. Rev. E **49**, 5158 (1994).
[51] E. R. Dufresne, D. Altman, and D. G. Grier, Europhys. Lett. **53**, 264 (2001).
[52] A. W. C. Lau and T. C. Lubensky, Phys. Rev. E **76**, 011123 (2007).